Advances in metalorganic vapor-phase epitaxy

by M. A. Tischler

Metalorganic vapor-phase epitaxy (MOVPE) has become a well-established technique for the epitaxial growth of lavers of III-V compound semiconductors since its introduction in 1968. Use has been made of the technique to produce such layers and associated devices to very demanding specifications. This paper describes MOVPE, followed by an overview of work at the IBM Thomas J. Watson Research Center on the technique, with emphasis on doping and selective epitaxy. Device applications are included to highlight the need to take into account the influence of materials and growth phenomena in order to produce optimum devices.

Introduction

Metalorganic vapor-phase epitaxy (MOVPE) and molecular beam epitaxy (MBE) are the two main crystal growth techniques currently used to grow epitaxial structures for III-V compound semiconductor devices. MOVPE and MBE can be used to produce heterostructures with very

[©]Copyright 1990 by International Business Machines Corporation. Copying in printed form for private use is permitted without payment of royalty provided that (1) each reproduction is done without alteration and (2) the *Journal* reference and IBM copyright notice are included on the first page. The title and abstract, but no other portions, of this paper may be copied or distributed royalty free without further permission by computer-based and other information-service systems. Permission to *republish* any other portion of this paper must be obtained from the Editor.

fine control of layer thickness, interface structure, material composition, and impurity concentration. These capabilities have resulted in new and improved devices such as modulation-doped field-effect transistors, solid-state lasers, and heterojunction bipolar transistors. In addition, structures for investigating quantum effects and dimensionally reduced systems are easily fabricated. The ability to conveniently fabricate such structures has had a significant impact on the fields of solid-state and device physics. It is precisely because of this wide-ranging impact that research in such crystal growth techniques continues.

This paper is divided into two sections: The first describes the MOVPE technique, while the second is an overview of work on the technique at the IBM Thomas J. Watson Research Center, emphasizing doping of III–V semiconductors and selective epitaxy. Selective epitaxy is a modification of the conventional growth technique which offers additional control over the deposition process in the lateral direction. Two major themes are stressed: First, the achievement of control of the structural and electrical characteristics of the material by developing an understanding of the growth process; second, the achievement of optimum device characteristics by developing an understanding of the effects of growth-and materials-related phenomena on device characteristics.

MOVPE technique

The MOVPE technique was first extensively developed by Manasevit in 1968 for the growth of III-V semiconductors [1]. The designation MOVPE is derived from the precursors for the column III metals, Ga, Al, and In,

which are supplied from metalorganic compounds; for example, a common gallium precursor is trimethyl gallium [TMGa, (CH₃)₃Ga]. In most applications the deposition is epitaxial with the structure of the single-crystal substrate upon which it is deposited. Polycrystalline or amorphous deposition will occur if single-crystal substrates are not used. In the general embodiment of the process, these column III metalorganic compounds react with hydrides of the column V elements at elevated temperatures to produce a III–V compound as follows:

$$MR_3 + XH_3 \rightarrow MX + 3RH$$
,

where M is a metal, X is a column V element (As, P, Sb), and R is an organic ligand such as CH_3 or C_2H_5 . This technique has also been used for the deposition of II-VI compounds. The most common precursors for the growth of GaAs are TMGa and AsH_3 through the overall reaction

$$Ga(CH_1)_3 + AsH_2 \rightarrow GaAs + 3CH_4$$
.

The mole fractions of these precursors in the reactor must be accurately controlled to be able to produce specific materials and structures. Device structures have stringent requirements for thickness, composition, impurity content, and interface characteristics, as well as the need for a high degree of uniformity of these characteristics over the entire deposition area. The electrical characteristics of such layers are directly related to their growth parameters. The MOVPE system, shown in Figure 1, is designed to precisely control the concentrations of all of the species in the reactor and provide uniform deposition characteristics. Electronic mass flow controllers regulate the concentration of gaseous precursors (i.e., hydrides and some dopants). The metalorganics, which are generally liquids, are transported by bubbling an inert gas such as H, through the container holding the liquid. Accurate and reproducible delivery requires control of the flow of H, through the liquid, as well as control of the source temperature and pressure. Abrupt changes in composition and dopant concentration are accomplished through the use of a vent-run manifold (not shown in figure) which can quickly direct the precursors either into the reactor for growth (run) or to the exhaust (vent). Abrupt interfaces are produced because the concentration of each species in the reactor is rapidly and controllably changed. High-vacuum construction techniques are used throughout the system, including the use of stainless steel tubing with welded or metal-to-metal fittings. This is required because of the reactive and toxic nature of the precursors and the need for a clean, oxygenfree growth environment.

Deposition takes place in the growth chamber, which is constructed of quartz, with the substrate placed on a heated susceptor (usually made of graphite and heated by rf induction). Upon entering the reactor, the precursors

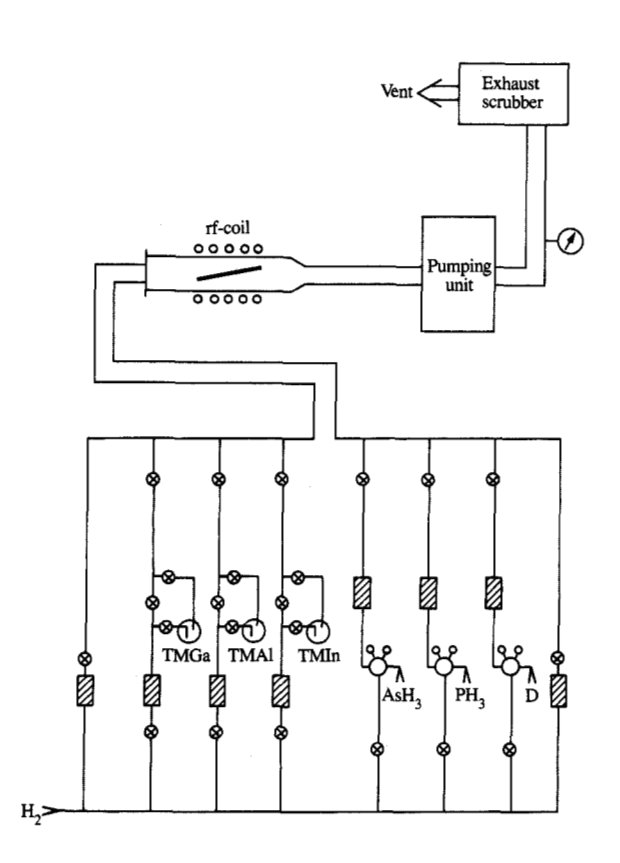


Figure 1

Schematic of a horizontal MOVPE system, showing both liquid (MO) and gaseous (hydrides and dopant) sources. The partial pressure of each species is controlled by an electronic mass-flow controller (cross-hatched boxes). The liquid species are transported to the reactor by flowing H_2 through the containers (bubblers) holding the liquid sources. A dopant source is designated as D. The pressure of each gaseous source is controlled by a regulator upstream of its mass-flow controller. The substrate is located on a tilted graphite susceptor which is heated by rf induction. The exhaust scrubber removes particulates and unreacted metalorganics and hydrides.

mix and may initially decompose in the hot region above the substrate. Deposition occurs on hot surfaces which include the substrate, susceptor, and portions of the quartz reactor. Reactor pressures vary from ~10 to 760 torr, with lower pressures generally resulting in improved uniformity. Reactor design is important because of its strong influence on the uniformity of the deposition and the capability of forming abrupt interfaces. Horizontal reactors, as shown in Figure 1, are well suited for research and development systems in which only a limited substrate area is required. High-capacity reactors are generally of the "barrel" design, in which the wafers sit nearly vertically on a

| Precursor | | | mposition range (°C) | Reference |
|----------------------|-----------------------------------|-------|----------------------------|-----------|
| | • | Start | Complete | |
| Trimethyl gallium | Ga(CH ₃), | 370 | 470 | [76] |
| Trimethyl gallium | Ga(CH ₃) ₃ | 400 | 580 | [3] |
| Triethyl gallium | $Ga(C_2H_5)_3$ | 220 | 330 | [76] |
| Trimethyl aluminum | Al(CH ₃) ₃ | ~330 | _ | [77] |
| Triethyl aluminum | $Al(C_2H_5)_3$ | ~200 | _ | [78] |
| Trimethyl indium | $In(CH_3)_3$ | 260 | 380 | [79] |
| Arsine | AsH, | 550 | 750 | [3] |
| Phosphine | PH, | <400 | 900 | [79] |
| Trimethyl arsine | As(CH ₃) ₃ | 425 | 650 | [59] |
| Tertiarybutyl arsine | $(C_4H_9)AsH_2$ | 240 | 480 | [59] |

barrel-shaped susceptor. The susceptor is rotated to improve the deposition uniformity. Commercial systems can hold over 50 two-inch-diameter substrates. The exhaust from the MOVPE system contains toxic material which must be properly treated, including filtering and scrubbing to remove particulates and unreacted hydrides and metalorganics.

Growth of III-V materials

◆ III-V materials

Compound semiconductors contain two or more elements having different vapor pressures. Thermal processing of these materials requires special attention to prevent surface decomposition. Above the congruent sublimation temperature T_{cs} , the anion element may evaporate at a higher rate than the cation in vacuo [2]. Because T_{cs} is generally lower than the growth temperature, an excess of the volatile species must be provided to prevent decomposition of the material. In the case of GaAs, $T_{cs} \sim 640$ °C. The vapor pressure of As over GaAs is appreciable at even lower temperatures, so that the GaAs surface must be stabilized with an arsenic overpressure when the process temperature is above $\sim 450^{\circ}$ C. The wide range of As activities allowed over the GaAs surface within the GaAs phase stability region prevents the buildup of As on the surface. Instead, it is incorporated as necessary to maintain stoichiometry of the growing film. Deposition begins when the column III precursors are introduced to the reactor along with the excess of the group V element. The growth rate is generally proportional to the mole fraction of the column III elements. The ratio of the mole fractions of the column V to column III species (V/III) is >1 during growth to provide the excess anion species required to stabilize the surface. Additionally, the decomposition of the column V hydrides (AsH, and PH,) is much less efficient than the column III

metalorganics, at normal growth temperatures, necessitating the use of a large V/III ratio in the reactor.

• Precursors

There are a wide variety of compounds which could serve as possible growth precursors. However, only a small fraction are suitable for use in the MOVPE process. Criteria for useful precursors include 1) a vapor pressure high enough to yield reasonable growth rates; 2) the ability to be sufficiently purified; 3) controlled interaction with other species or materials in the growth ambient; 4) minimal intrinsic incorporation of unwanted impurities (most commonly carbon from the metalorganics): 5) controlled decomposition at growth temperatures, and 6) high stability during storage. Common precursors along with their pyrolysis characteristics are listed in Table 1. The most widely used anion precursors are the hydrides of As and P: AsH, and PH,. As shown by the table, these have relatively high decomposition temperatures which lead to a low efficiency of use. In addition, the hydrides are extremely toxic, and special care and equipment must be used to ensure safe storage, operation, and eventual disposal of these materials. These concerns have prompted a great deal of research on alternate As and P precursors, some of which are included in the table. In general these alternate sources are liquids, which, while not necessarily being less toxic than the hydrides, are considered less hazardous because of their lower vapor pressure. The cation precursors are in the form of metalorganic compounds, which are usually liquids. Such compounds are very reactive and also require careful handling.

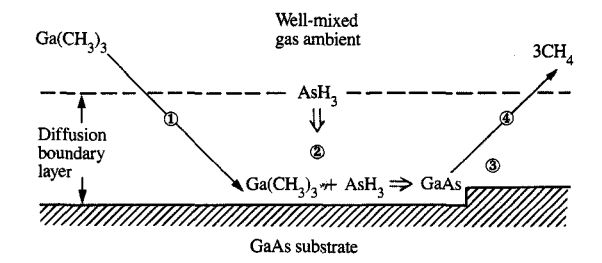
• Deposition reaction

The deposition reaction is driven by a supersaturation of the constituents of the compound in the gas phase. These elemental species are supplied by the decomposition of precursor molecules. In recent years a great deal of work has gone into understanding and modeling the chemistry and decomposition of these precursors. Important aspects of the work include the determination of the temperature dependence of the primary decomposition pathways which lead to growth, as well as the determination of reaction by-products and their participation, if any, in this process. Catalytic effects brought on by other precursors, the substrate, or materials in the reactor are also important. The decomposition temperature of AsH₂, for example, is reduced in the presence of a GaAs surface [3]. This information is necessary to the understanding of the growth process and incorporation mechanisms of intentional and unintentional impurities. An understanding of these mechanisms then aids in the design and choice of precursors tailored for specific characteristics.

A schematic description of the growth of a GaAs layer using TMGa and AsH₃ is shown in Figure 2. The latter is

present in excess to stabilize the GaAs substrate; hence, the growth rate is determined by the TMGa concentration. Growth proceeds through a series of steps: The TMGa diffuses from the gas stream to the substrate region, precursor decomposition occurs near or on the substrate. the new material is incorporated into the growing layer, and the reaction by-products are removed. The growth rate is determined by the slowest of these steps. The growth temperature is typically well above the decomposition temperature of the column III metalorganic compounds, so their decomposition is not usually the rate-limiting step. The column V species are present in such excess that their decomposition is not rate-limiting. The incorporation of GaAs into the epitaxial layer, and desorption of reaction by-products, occurs rapidly at typical growth temperatures. The mass-transport or gas-phase diffusion of the column III precursor to the substrate is therefore generally observed to be the rate-limiting step under typical growth conditions.

The precursor used to supply a particular element to the growing layer follows one or more decomposition reaction pathways which lead to eventual incorporation. As an example of one step in the process, TMGa could lose a methyl radical (CH₂) to become dimethyl gallium. The CH₂ radical could react with a hydrogen to form CH₄. The actual pathway for incorporation is a complex multistep process. Each step in the reaction pathway can consist of many different types of reactions. These can be homogeneous (in the gas phase) or heterogeneous (involving a surface) reactions, and can occur unimolecularly (by themselves, e.g. bond breaking due to heating) or bimolecularly (interaction between two species). For example, the parent precursor could partially decompose in the gas phase, be adsorbed on the surface, react with another species, and finally be incorporated. There have been a large number of studies to elucidate these reactions, in order to gain a better understanding of the growth process [3-10]. Many of these studies utilized experimental conditions which were different from those used in working reactors; in order to obtain useful information, care must be taken in the interpretation of the data. In recent years the design of such studies has become quite sophisticated, for example employing isotopically labeled precursors to aid in tracking of the reaction by-products. For example, the role of the H, carrier gas has been investigated by replacing it with D [5]. Another technique has been to sample the gas through a pinhole in the susceptor in a "normal" reactor [7], thereby examining the gas phase just above the growing layer. These studies have greatly increased the understanding of the growth process, and have provided insight into tailoring growth conditions or precursors to achieve specific material characteristics.



- 1 Diffusion to substrate region
- Decomposition near or on substrate
- 3 Incorporation into growing layer
- Removal of reaction by-products

Figure 2

Schematic of the steps in the growth of a GaAs layer, using TMGa and AsH₃. The growth rate is determined by the slowest of the following sequential steps: diffusion of the TMGa from the gas stream to the substrate region, decomposition of the precursor near or on the substrate, incorporation of the new material into the growing layer, and removal of the reaction by-products. From [22], reproduced with permission.

The complete growth process including chemical, thermal, and hydrodynamic effects is extremely complex, and hence difficult to model accurately [3, 9–13]. A number of simple models have been developed which are based on the mass transport of a species through a concentration boundary layer to the substrate as the rate-limiting step [14]. This boundary layer can be thought of as a gas-phase region which is depleted of the growth-rate-limiting constituent. At the leading edge of the deposition zone, the gas is homogeneous. However, as the gas passes over the substrate, more and more material is depleted from the gas phase to form the deposited layer. Therefore, the thickness of this boundary layer δ_d increases with distance along the gas flow direction, and can be expressed [15] as

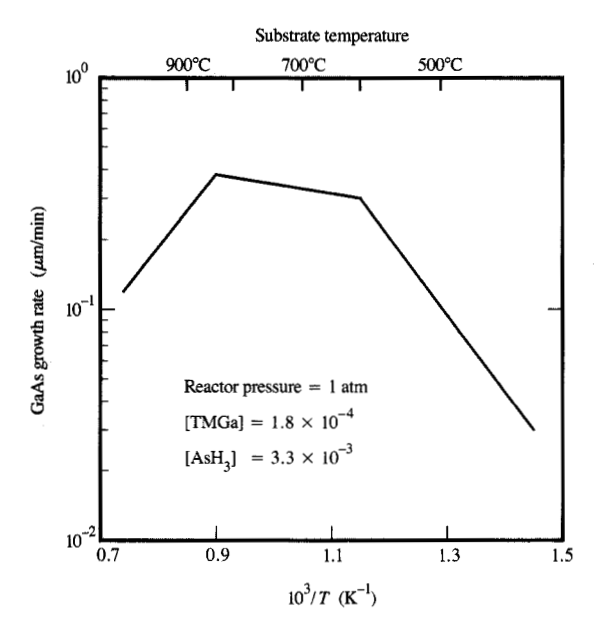
$$\delta_{\rm d} = 3 \left(\frac{D}{\nu}\right)^{\frac{1}{3}} \left(\frac{\nu\ell}{V}\right)^{\frac{1}{2}},$$

where D is the diffusion coefficient, ν is the kinematic viscosity, ℓ is the distance down the reactor, and V is the velocity of the gas in the reactor. The flux to the substrate, which determines the growth rate, is then given by

$$F = -D \frac{dC}{dy} \bigg|_{\text{surface}} \simeq -D \frac{C_0}{\delta_d},$$

where C_0 is the initial concentration of the rate-limiting species in the gas phase. It is evident from this expression





GaAs growth rate as a function of substrate temperature T, using TMGa and AsH_3 . Growth is usually carried out in the mass-transport-limited (temperature-independent) regime. From [22], reproduced with permission.

that the growth rate is linearly proportional to the concentration of the rate-limiting species, e.g., the column III precursor. In this simple model, the growth rate is predicted to be nonuniform, decreasing along the length of the reactor as $\delta_{\rm d}$ increases. To achieve a uniform growth rate within the context of this model, $\delta_{\rm d}$ is kept constant by causing V to increase along the length of the susceptor. This is done by tilting the susceptor to decrease the cross-sectional area of the reactor.

The growth rate and uniformity are also affected by the fluid-thermal environment in the reactor. The simple concept of a concentration and thermal boundary layer is not sufficient for accurate modeling of the growth rate and uniformity of deposition and doping in realistic reactors [16-20]. There are several complicating factors in the fluidthermal environment. These factors arise from the coupling of the heat and momentum transport in the reactor. Forced convection drives the gas through the cool regions of the reactor upstream of the hot susceptor. Most reactors are designed to establish laminar flow within this region. The gas rapidly expands as it flows over the hot susceptor in accordance with the ideal gas law. This rapid gas-phase expansion can set up a return flow in the reactor, bringing partially reacted gases upstream with a subsequent recirculation into the input stream. The presence of large

thermal gradients between the hot susceptor and the cool walls of the reactor can also lead to the formation of thermal convection cells within the reactor. These cells also serve to recirculate partially reacted gases back into the input gas stream. Such recirculations can degrade both growth rate uniformity and materials properties. They can also prevent the rapid switching of the reactants in the gas stream, thus impeding the formation of abrupt metallurgical and electronic junctions.

Much of the recirculation can be minimized or even eliminated through proper reactor design [11, 16, 18, 20]. In addition, reduced reactor pressures are also used to remove the thermally driven convection cells [18]. The Grashoff number, which is strongly dependent on pressure $(Gr \propto P_{\text{reactor}}^2)$, is used to characterize the tendency of a fluid flow system to form thermal convection cells [21]. Thus, reducing the reactor pressure from 760 torr to 76 torr accomplishes a hundredfold decrease in the driving force for thermal recirculation. Accurate modeling of these fluid-flow effects which can predict such complicated behavior requires the application of numerical modeling techniques. The particular thermal boundary conditions chosen in the modeling have a strong influence on the predicted growth rate and uniformity. Realistic modeling of these systems is extremely complex because of the strong nonlinear characteristics of the Navier-Stokes equations used to describe the fluid-flow field [11, 18, 21]. The ideal gas law required to describe the flow medium has an inverse dependence of the gas density on the local temperature. Such nonlinear problems can have multiple solutions depending on the initial conditions used in developing the solution. These modeling difficulties have limited the development of working descriptions of actual MOVPE systems to the research stage.

The dependence of the growth rate of GaAs on substrate temperature [22-24] is shown in Figure 3. Typically, growth is carried out in the intermediate, temperatureindependent regime. This is the mass-transport-limited regime, as described above, in which the rate-limiting step is diffusion of the column III species to the substrate and the growth rate is linearly dependent on the concentration of the column III species. The near temperatureindependence of the growth rate is a result of the small change in gas-phase diffusion coefficient over this temperature range. In the low-temperature regime, the growth is kinetically limited by one of the many possible chemical reactions, and the growth rate decreases with temperature. Under such temperature-activated conditions, the growth rate is controlled by the adsorption and pyrolysis of the precursor species on the substrate. Surface processes now influence the rate-limiting step, resulting in a growth rate which varies with substrate orientation. The growth rate also decreases at much higher temperatures. This can be caused by gas-phase depletion of the growth

nutrients prior to reaching the substrate or by desorption of the Ga species from the surface [22–24]. It is important to keep in mind that this simple description does not begin to reveal the complexities of the actual deposition reactions, including heterogeneous and homogeneous reactions which are dependent on system pressure, temperature and hydrodynamic profiles, and residence time of the gases in the system.

• Electrical characteristics

The electrical characteristics of III–V semiconductor layers depend strongly on the conditions under which they are grown. Many factors can affect the decomposition and incorporation characteristics of electrically active impurities and defects. Growth temperature and pressure, mole fractions of the individual precursors in the gas phase, and ratios of certain gas-phase mole fractions (most notably the V/III ratio) can all influence impurity incorporation. Unintentional doping of the material is determined in part by the particular combination of precursors used, and their interaction with the growth ambient. In spite of these complex dependencies, growth process windows exist in which virtually all III–V and II–VI compounds can be grown in high-purity form.

The most common donor elements used in the MOVPE of III-V semiconductors are silicon, sulfur, selenium, tin, and tellurium; common acceptors include carbon, zinc, and magnesium. These can be intentionally or incidentally introduced to modify the electrical characteristics of the semiconductor. Unintentional impurities can be categorized as either resulting from contaminants in the precursors or growth environment, or those that are intrinsic to the growth process. Carbon is the main impurity that is intrinsic to the growth process and has its source in the organic ligands attached to the metals. The carrier concentration in nominally undoped GaAs is especially sensitive to the V/III ratio, as shown in Figure 4. As can be seen, the carrier type changes from p- to ntype as the V/III ratio increases. This behavior results from a decrease in the electrically active carbon concentration in the solid as the V/III ratio is increased. To reduce the carbon concentration in the solid, the CH, $(x \le 3)$ radical must combine with an H on or near the surface to form the nonincorporating species CH. Changing the ambient from H, to He has been shown not to have an effect on the carbon concentration under typical growth conditions [25]. The primary source of H for this reaction is therefore the AsH₁. The electrical behavior with changing V/III ratio can now be understood through the mechanism of carbon removal by the AsH, [25]. At low V/III ratios, there is relatively little AsH, present, so the efficiency of H combining with the CH, radicals is low. These radicals can then further decompose or react with

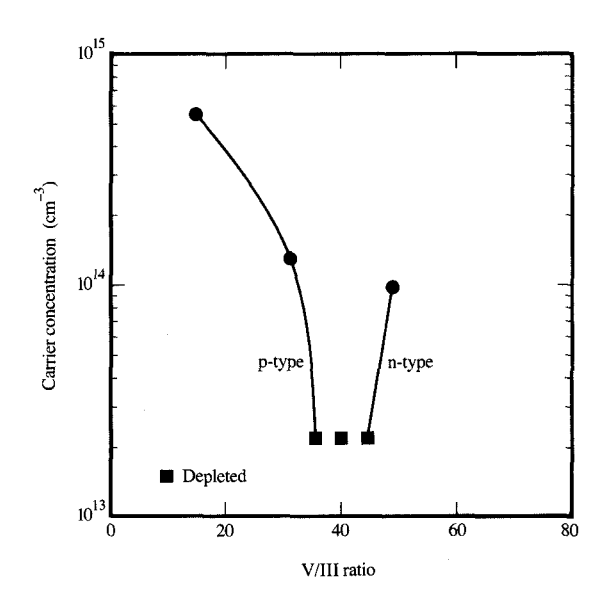
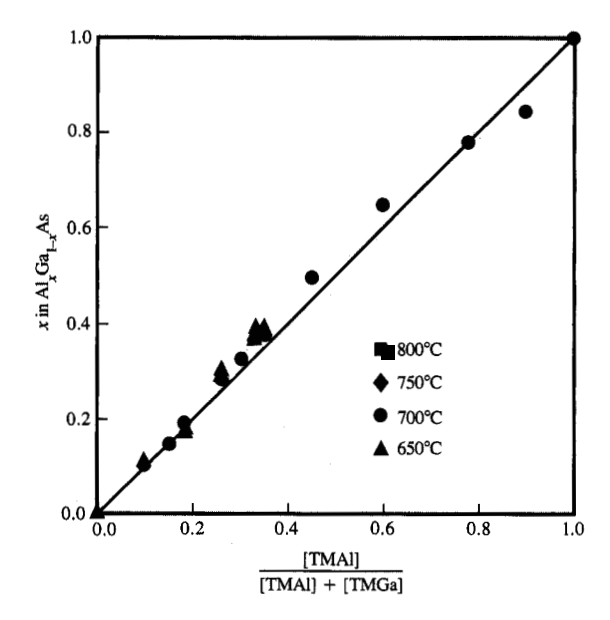


Figure 4

Carrier concentration in GaAs grown at 625°C and 78 torr, as a function of V/III ratio.

other growth constituents on the surface, leading to carbon incorporation. As the V/III ratio is increased, more AsH. and thus H is present, and the carbon incorporation decreases. The material can become highly resistive when the carbon and unintentional donor concentrations are approximately equal. A further increase in the V/III ratio results in donor-dominated conduction, and the material becomes n-type. Germanium originating as a contaminant in the AsH, has been suggested as the dominant donor. The n-type carrier concentration then increases because the Ge concentration increases with the AsH, concentration. The V/III ratio at which the conductivity changes type is dependent on the purity of the precursors as well as the AsH, decomposition efficiency. The carbon concentration is also affected by other variables such as the growth temperature, pressure, and substrate orientation [22].

The variation in conductivity type with V/III ratio in undoped GaAs provides an example of how strongly the growth process can affect the electrical characteristics of the material and the growth process. In many devices, use is made of an undoped layer beneath the active portion of the device. In a metal-semiconductor field-effect transistor (MESFET), for example, the conductivity type and concentration of such a layer can have a large effect on electrical characteristics [26]. For example, the presence of a p-n junction below the channel changes the electric field



Aluminum arsenide concentration x in Al_xGa_{1-x}As as a function of mole fraction ratio [TMA1]/([TMA1] + [TMGa]) in the gas phase.

within the channel region, and thus the threshold voltage of the device. A p-type buffer acts to "cut off" the tail of the n-type channel implant, improving the output conductance and subthreshold leakage of the MESFET [27]. Conversely, an n-type buffer degrades these characteristics.

The discussion has thus far concentrated on the use of

Growth of ternary alloys

MOVPE to grow layers of the binary compound GaAs. The wide applicability of III-V materials derives from their suitability for forming heterostructures composed of layers with different structural, electrical, and optical characteristics. The materials system most widely used has been the Al₂Ga₁₋₂As/GaAs system, in which the entire range of compounds from x = 0 to 1 can easily be grown. The alloy bandgap increases and the dielectric constant decreases with increasing AlAs composition. Heterostructures can be used to confine carriers, as in quantum wells and two-dimensional electron gas systems, or to confine photons, as in optical waveguides and semiconductor lasers. The Al₂Ga₁₋₂As alloy system is unique in that the two binary endpoints are very closely lattice-matched; the lattice mismatch between GaAs and AlAs is only 1.28×10^{-3} at room temperature. This

means that any composition alloy can be grown with reasonable thicknesses on GaAs, without the formation of misfit dislocations. This is in contrast to other common heterostructure systems such as InP/In, Ga, As and In, Ga, As/GaAs, which are respectively lattice-matched at only one composition or not lattice-matched at all. Latticemismatched structures can also be grown; these greatly increase the available heterostructure combinations. There is a critical thickness beyond which misfit dislocations are generated, for a given mismatch between the layers [28]. Dislocations and other structural imperfections are generally avoided because they adversely affect the electrical or optical properties of the semiconductor structure. Below the critical thickness, the lattice constant of the epitaxial layer is strained to match that of the substrate, and high-quality material with no misfit dislocations can be grown. The strain induces a tetragonal distortion in the lattice which gives rise to changes in the band structure [29], thus providing a means for modifying the electrical and optical properties of such layers.

Al₂Ga₁₋₂As is most widely grown using the precursors TMGa and trimethyl aluminum (TMAl). Because these have similar decomposition characteristics and diffusion coefficients, the growth of Al, Ga,-xAs is relatively straightforward and can be thought of as the simultaneous growth of GaAs and AlAs. The growth rate of each binary, in the mass-transport-limited regime, is determined by the diffusion of the respective species to the substrate. The growth rates are dependent, to first order, on the concentrations of these precursors. The aluminum concentration in the solid is given by the ratio of the mole fraction of TMAl to the sum of the TMGa and TMAl mole fractions, as seen in Figure 5. The slight bowing of the experimental data is a result of the differences in diffusion coefficients between TMGa and TMAl. The ratio of D_{TMAL} to D_{TMGa} determined from this bowing is approximately 1.2. Al incorporation rates have been noted to be higher when TMGa is replaced by triethyl gallium (TEGa). The lower TEGa pyrolysis temperature makes it more susceptible to gas-phase depletion effects, and the lower diffusion coefficient reduces the growth rate of GaAs, thus increasing the Al concentration in the solid. Similar effects are seen when TMAl is replaced by triethyl aluminum (TEAl). The Al composition in the solid is reduced as a result of upstream decomposition of TEAl and its smaller diffusion coefficient. The low decomposition temperatures of the ethyl-based precursors also lead to increased nonuniformities in thickness and composition.

The elements in columns III and V can be used to produce a wide variety of ternary alloys. These can be divided into those with mixed column III elements, $III_xIII'_{1-x}V$, and mixed column V elements, $IIIV_xV'_{1-x}$. In general, alloys of the form $III_xIII'_{1-x}V$ are more straightforward to produce. Column III precursors for each

element can usually be found with similar decomposition and diffusion characteristics. The composition of the solid in this case is directly proportional to the ratio of the column III precursors in the gas phase, and acceptable thickness and compositional uniformity can be maintained. If the characteristics of the two precursors are very dissimilar, the solid composition may not be directly proportional to the ratios in the gas phase, and the thickness and compositional uniformity are degraded. An example of this is the growth of the mixed column V alloy $GaAs_{1-r}P_r$. The ratio of PH₃ to AsH₃ in the gas phase is typically much larger than the ratio of P to As in the solid [30], because the pyrolysis temperature of PH, is much higher than that for AsH, (see Table 1). Additionally, the uniformity is more dependent on the thermal profile over the entire deposition area in these cases. Quaternary alloys, with both mixed column III and V elements, have also been grown. These multicomponent systems possess a broad range of bandgaps at a single lattice constant. $In_xGa_{1-x}As_{1-y}P_y$, which is of current technological interest for both optical and electronic applications, can be grown lattice-matched to InP with bandgaps ranging from 0.7 to 1.34 eV. These bandgaps cover the low-absorption regions at 1.3 and 1.55 µm in optical fibers. Such multicomponent systems are more difficult to deposit because of the high degree of control over the growth process required to achieve lattice match.

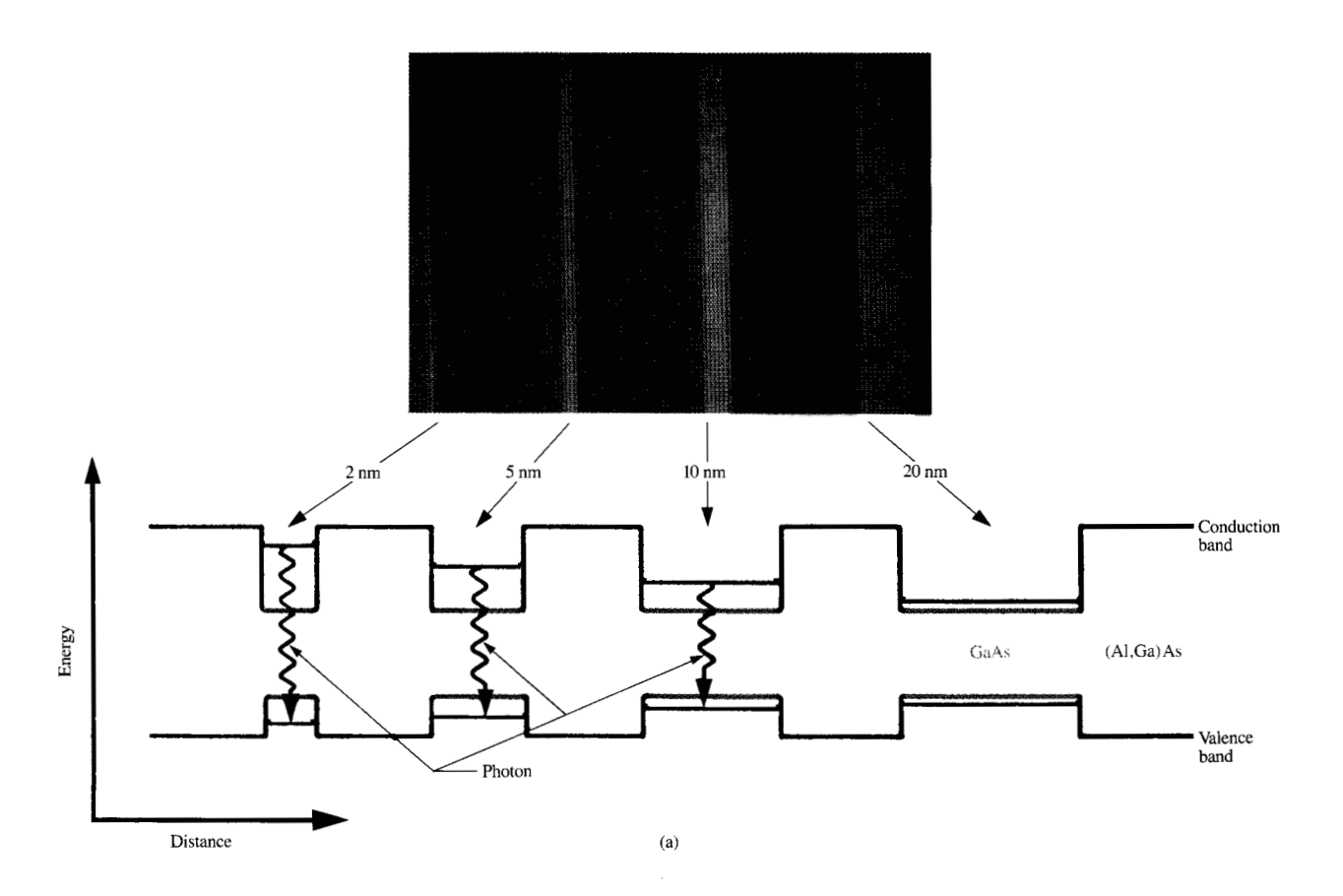
Heterostructures

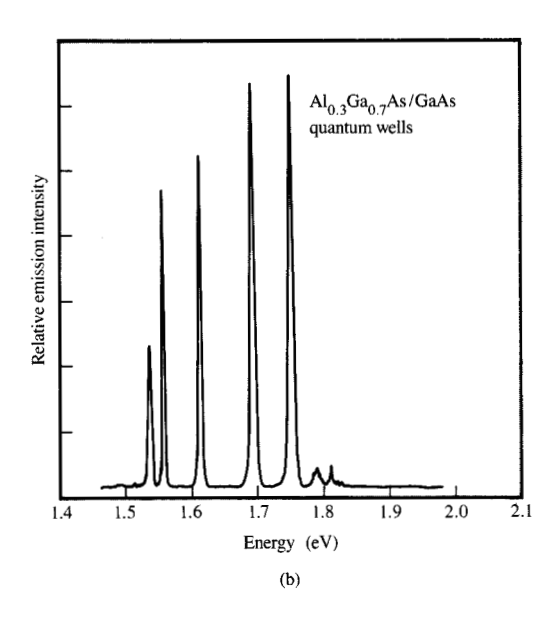
In addition to control of the composition and thickness of individual layers, control of the composition profile at a heterojunction interface is also very important in device structures. The performance of heterostructure devices, such as lasers and heterojunction bipolar and twodimensional gas transistors, relies on the achievement of specific electronic band structures, which are directly related to the compositions and dopant profiles at the interfaces. The structure of heterointerfaces has often been inferred from photoluminescence (PL) [31, 32] and transmission electron microscopy (TEM) measurements. Both of these types of measurements yield information which is spatially averaged over a distance of one to several hundred angstroms. In the case of PL measurements, the luminescence from quantum-well structures is representative of the interfacial composition averaged over an exciton diameter, which is typically about 100-200 Å. Additionally, conventional PL spectra only reveal information associated with the lowest or ground state of the exciton in the well. There is not a unique correspondence between the spectral peak position and the compositional changes through the heterointerface. Nonetheless, the narrowness of the PL peak associated with the quantum well gives a qualitative measure of the uniformity of the interfaces in the structure. PL excitation

spectroscopy can be used to obtain information on the higher-lying states in the well. TEM studies, which yield lattice images, have also been used to infer the physical and chemical structure across an interface. A TEM image is formed from a sample of finite thickness, which inevitably leads to the spatial averaging of the compositional information throughout its thickness. Recently, statistical and image processing techniques have been applied to the study of TEM images with the objective of obtaining chemical information across the heterointerface [33]. Such studies have indicated that while the average compositional variation in the plane of a quantum well may be minimal, there are fluctuations in composition over 2-3 atomic layers in the growth direction. These lateral fluctuations are of the order of ~10 Å. Such fluctuations do not influence the PL peak position or spectral linewidth, often a figure of merit for a quantum well, but do indicate that these heterointerfaces are not atomically smooth [33]. The development of highresolution X-ray diffraction techniques has also been applied to the study of superlattices and quantum wells. One advantage of this technique is that X-ray diffraction spectra can be quantitatively modeled [34].

A series of quantum wells consisting of GaAs wells and larger-bandgap Al_{0.30}Ga_{0.70}As barriers grown by low-pressure MOVPE [35] are shown in Figure 6. Part (a) shows a schematic drawing and TEM micrograph of a structure containing four quantum wells ranging from about 20 to 200 Å in width. Part (b) shows a PL spectrum from a similar structure containing five wells ranging from about 15 to 155 Å in width. The well and barrier layers (GaAs and Al_{0.30}Ga_{0.70}As, respectively) are clearly distinguished in the micrograph, demonstrating the ability to produce extremely thin layers with interface widths of the order of several monolayers. In this case, the thinnest GaAs well is only 20 Å wide. The PL peaks corresponding to the wells have narrow widths, which is characteristic of uniform (to within several monolayers in width) interfaces.

Other heterostructures involving mixed column III elements, as well as those incorporating mixed column V elements (InP/In, Ga_{1-r}As), can also be grown. Mixed column III heterostructures can generally be grown with more abrupt interfaces, because the growing layer can be left under the common column V flux while the unwanted column III precursor is purged from the reactor. This cannot be done in the case of mixed column V heterostructures, because a column V overpressure is continually required to prevent surface decomposition. Grading of the interface can also occur when the column V fluxes are switched, even if no growth is occurring. X-ray diffraction characterization of (In,Ga)As/InP materials has indicated a basic asymmetry between InP-(In,Ga)As and (In,Ga)As-InP interfaces [34]. These undesired features can affect the electrical and optical characteristics of a





(a) Schematic and TEM micrograph of an MOVPE-grown GaAs/AlGaAs structure containing four quantum wells, from [35(b)], reproduced with permission. Copyright 1988 by the AAAS. (b) Photoluminescence at 4~K from a similar quantum-well structure.

device as well as causing possible physical degradation by the formation of misfit dislocations.

Intentional doping

The quantum wells described in Figure 6 demonstrate the ability to produce abrupt compositional interfaces in the AlGaAs/GaAs system. In some cases, spatially controlled or abrupt dopant profiles are required—for example, in the fabrication of two-dimensional electron gas (2DEG) structures and heterojunction bipolar transistors. Creating an abrupt dopant profile can be more difficult than creating an abrupt composition profile for a number of reasons. This is because the optical and electrical characteristics are generally less affected by small amounts (<1%) of major constituents (for example, 1% Al in GaAs) than by a similar level of unwanted dopants. Also, the diffusion coefficients of major constituents, for example Ga in AlGaAs, are much less than for dopants.

A controlled dopant profile requires first that the dopant be placed in the structure accurately, and second that its subsequent movement be minimized. The placement of the dopant is governed by the precursor used, its interaction, if any, with the growth system, and the vapor pressure of the element itself. Dopant redistribution is controlled by diffusion of the element in the host material. Many dopant precursors exhibit what has been termed a "memory effect," a slow approach to steady state after the dopant is introduced. Similarly, when the dopant is turned off, the concentration, instead of falling abruptly, decreases slowly. These transients are primarily caused by adsorption and desorption of the dopant species on the interior surfaces of the system. When the dopant is initially introduced, these internal surfaces act as a sink for the precursor, and some time is required for these sites to become saturated. The surfaces later act as unintentional sources after the dopant source is shut off, by desorbing the previously adsorbed species. If the solid-state diffusion coefficient of the dopant is large, the dopant profile changes during subsequent growth, even if the dopant species is initially placed as desired. Thus, the ideal dopant would have no memory effect and a low diffusion coefficient. High electrical activity, comparable to the metallurgical concentration of the dopant, is typically required. Ideal dopant sources have a linear or sublinear dependence on the mole fraction of the precursor in the gas phase, and are not sensitive to other growth conditions such as temperature, pressure, or V/III ratio. It should be noted that concerns of memory effect and diffusion also apply to major constituents. For example, TMAl is reported to adsorb on silica [36]; however, as mentioned above, the addition of very small amounts of major constituents generally has a relatively small effect on electrical characteristics.

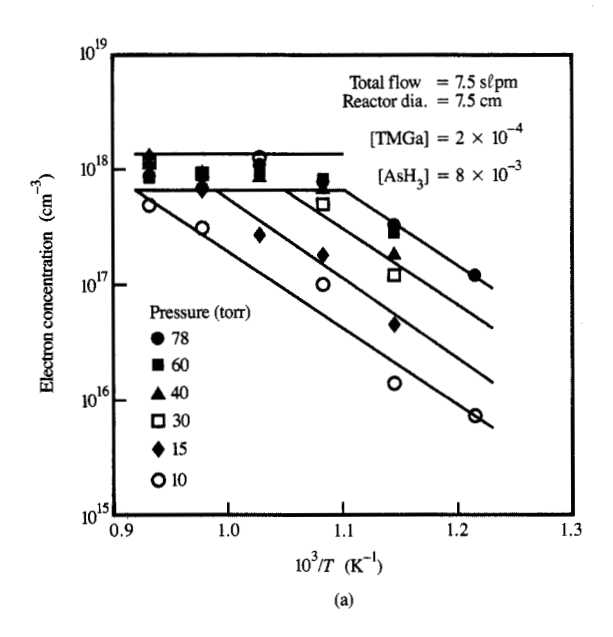
• Donors

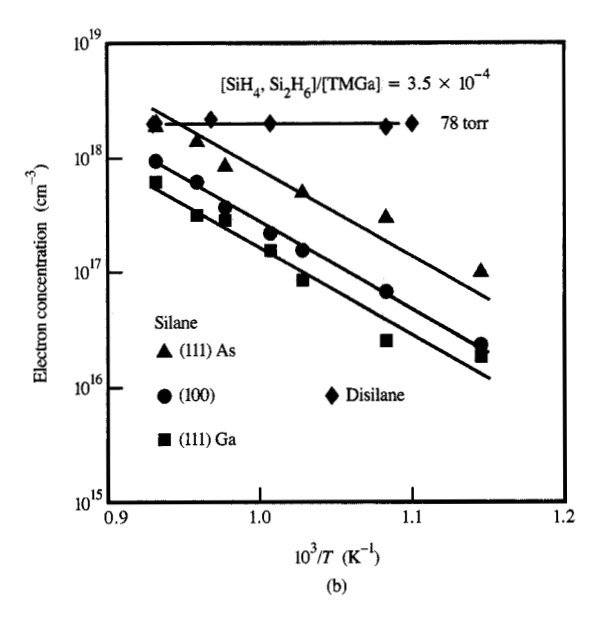
A large number of elements have been used as donors in III-V materials, including Si, Sn, and Ge from group IV, and S, Se, and Te from group VI of the periodic table. Si, Sn, and Ge, while amphoteric, are all incorporated as donors in the MOVPE technique. Sn, delivered either from $Sn(CH_3)_4$ [37, 38] or $Sn(C_3H_5)_4$ [39-41], is of interest because it can provide high electron concentrations [38], $>1 \times 10^{19}$ cm⁻³. Ge in the form of GeH₄ has not seen extensive use [42]. The column VI dopants are supplied as hydrides in the case of S and Se (H,S [43] and H,Se [44, 45]) and as metalorganic compounds in the case of Te [46-48]. The incorporation of these dopant elements decreases with increasing growth temperature and increasing V/III ratio. The decrease with growth temperature is a result of the high vapor pressure of these elements. In addition, they are characterized by a fairly strong memory effect, which makes production of abrupt dopant junctions difficult.

The donor which most closely approaches the ideal criteria listed above is Si, delivered from the precursor Si,H₆ [22]. The Si incorporation is directly proportional to the Si₂H₆ mole fraction up to concentrations of about $2 \times 10^{20} \ \text{cm}^{-3}$. The maximum realizable electrical carrier concentration is, however, only $5-8 \times 10^{18}$ cm⁻³. Si incorporation from Si₂H₆ is independent of growth temperature for pressures ≥60 torr [49], as shown in Figure 7(a). As the pressure is lowered, the range of this temperature-independent region decreases. The Si incorporation from another silicon source, SiH4, is strongly dependent on the growth temperature and substrate orientation, as seen in Figure 7(b). A strong temperature dependence is generally undesirable, since small changes or nonuniformities in temperature are mirrored in the carrier concentration. The different incorporation characteristics of these two precursors arise from the lower thermal stability of Si₂H₆, which appears to react with the AsH, at normal growth temperatures, forming an intermediate compound, SiH, AsH, [49]. The balance between the in situ generation and mass transport of this compound leads to the desired temperature-independent doping behavior. Because homogeneous SiH, pyrolysis is quite slow at typical growth temperatures, Si incorporation from SiH, is kinetically limited, as evidenced by the dependence on growth temperature and substrate orientation. Both of these precursors exhibit little memory effect, and the diffusion coefficient of Si in GaAs is quite low, making it ideal for use in structures which require abrupt donor profiles.

• Acceptors

The elements Be, C, Cd, Mg, and Zn have all been used as acceptor dopants in MOVPE. Among them, C, Mg, and Zn are the most commonly used, Cd [50] and Be [51] less so





(a) Silicon incorporation in GaAs using a Si_2H_6 source, as a function of pressure and the reciprocal of growth temperature. (b) Silicon incorporation in GaAs using Si_2H_6 and SiH_4 sources, as a function of substrate orientation and the reciprocal of growth temperature. The lines in both parts serve as an aid to interpretation. Part (b) from [22], reproduced with permission.

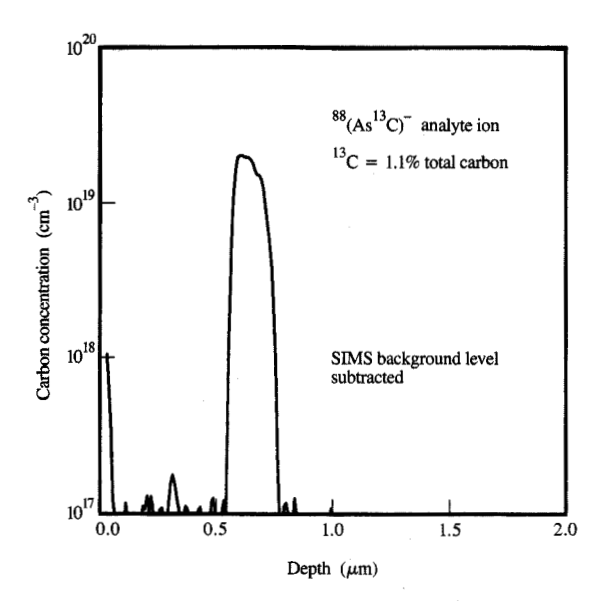


Figure 8

SIMS profile of a buried carbon-doped GaAs layer. The profile was found to be unchanged after annealing at 920°C for one hour. From [55], reproduced with permission.

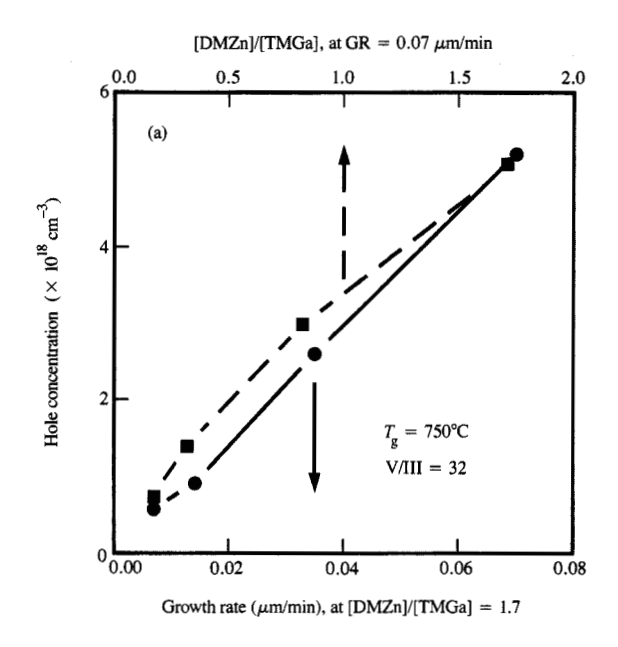
(in the case of Be, because of its toxicity). Mg is supplied in metalorganic forms: bis(cyclopentadienyl) magnesium, $Mg(C_5H_5)_2$ [52, 53], and bis(methylcyclopentadienyl) magnesium, $Mg(C_5H_4CH_3)_2$ [54]. The incorporation of Mg and Cd decreases with increasing growth temperature (above some temperature) and is characterized by a memory effect. At this time there are no acceptor dopants that have all of the desirable characteristics of Si_2H_6 . Carbon probably comes the closest, but, like Zn and Mg, has a strong temperature dependence to incorporation.

Carbon is the dominant unintentional acceptor in GaAs and Al Ga, As, and recently it has been used as an intentional dopant [55, 56]. There are two major advantages of carbon over zinc: the absence of a memory effect, and a lower diffusion coefficient. Abrupt carbon doping profiles are thus easily achieved, as illustrated by the secondary ion mass spectrometry (SIMS) profile of a carbon-doped spike shown in Figure 8. The same abrupt carbon profile was found in the "as-grown" layer and after annealing for one hour at 920°C. The diffusion coefficient for carbon in GaAs [57] is $\approx 10^{-16}$ cm²/s at 825°C. The structure shown in the figure was produced by growing the carbon-doped layer with TMAs instead of AsH, [55]. The TMAs provides As for GaAs growth and carbon as the acceptor. Acceptor doping is terminated by adding AsH, to the reactor. Because AsH, can be rapidly introduced into

the reactor, the dopant profile can be made extremely sharp. TMAs does not provide the atomic hydrogen necessary to prevent carbon incorporation (as described earlier) and thus permits enhanced carbon incorporation. The addition of AsH, provides atomic hydrogen, which very efficiently scavenges the methyl radicals from both the TMGa and TMAs, resulting in very little carbon incorporation. Intermediate amounts of carbon can be introduced by appropriate mixtures of TMAs and AsH₃. The electrically active carbon concentration is temperature-dependent, increasing as the temperature is reduced. High carbon concentrations are characteristic of many AsH, substitutes, which limits their use to situations where this is desirable or not a concern. The one AsH, substitute which does not exhibit high carbon concentrations is tertiarybutyl arsine [58, 59]. CCl, has also been successfully used as a carbon source. The temperature dependence of the resulting carbon incorporation is different from that of TMAs [56]. For CCl, the incorporation increases monotonically with temperature, whereas for TMAs, a minimum occurs at about 650°C.

The zinc precursors dimethyl zinc (DMZn) and diethyl zinc (DEZn) have been widely used [60, 61] despite their exhibiting strong temperature-dependent incorporation as well as memory effects. DEZn has a pyrolysis temperature that is much lower than normal growth temperatures, which results in gas-phase depletion and nonuniform carrier concentrations. These effects are somewhat reduced when use is made of DMZn, which has a slightly higher pyrolysis temperature. The dependence of the hole concentration in GaAs on the mole fraction ratios of DMZn and TMGa ([DMZn]/[TMGa]) is shown in Figure 9(a). The efficiency of DMZn is quite low compared to SiH₄ or Si,H₆, as can be seen from the high [DMZn]/[TMGa] ratios. In addition, the relationship is not linear, and begins to show some signs of saturation at high hole concentrations. The dependence of carrier concentration on the reciprocal of growth temperature for DMZn is shown in Figure 9(b). As can be seen, the zinc incorporation is constant at low temperatures, but decreases above ~600°C. At high temperatures, the zinc evaporates off the surface before becoming incorporated. The zinc concentration increases with growth rate, as seen in Figure 9(a), because deposited zinc is trapped by subsequently deposited GaAs, reducing the effective evaporation rate. This behavior is in direct contrast to that of SiH₄ and Si,H₆, in which the carrier concentration is inversely proportional to the growth rate.

The diffusion of zinc is a complex process, which has been generally described using a substitutional-interstitial model [62–68]. In this model the solubility of zinc interstitials (Zn_1) is very low compared to substitutional zinc (Zn_S) (referred to the column III sublattice), but the



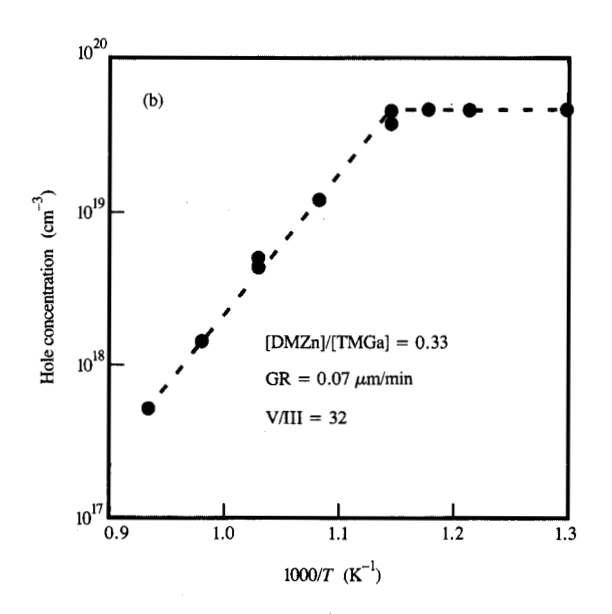
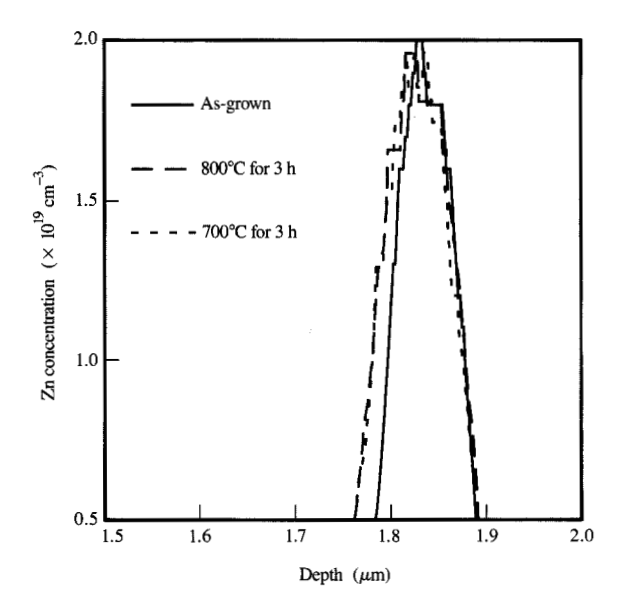


Figure 9

(a) Hole concentration in GaAs, using DMZn as the acceptor precursor, shown as a function of [DMZn]/[TMGa] and growth rate. (b) Hole concentration in GaAs using DMZn as the acceptor precursor, shown as a function of the reciprocal of growth temperature. From [40], reproduced with permission.

diffusion coefficient of Zn_l is so much larger than that of Zn_S that the presence of the latter may be neglected. Diffusion occurs when zinc transfers from a substitutional



SIMS profile of a zinc-doped GaAs layer sandwiched between undoped GaAs layers; as-grown, and after annealing for three hours at 700 and 800°C. From [69], reproduced with permission.

to an interstitial site. The zinc diffusion coefficient is determined by the ratio of interstitial to substitutional zinc. Interstitial zinc is produced by reactions with defects in the crystal; for example, zinc can transfer sites through the formation and annihilation of gallium vacancies and interstitials. The situation is complicated by the fact that the solubility of charged defects is affected by the position of the Fermi level in the host crystal [62, 68]; thus, the doping type and concentration also affect the diffusion coefficient. This leads to a concentration-dependent diffusion coefficient, which is manifested by steeper concentration gradients than are obtained with a concentration-independent diffusion coefficient.

The diffusion coefficient of zinc, in structures in which the zinc does not communicate with the surface, is much lower than typical values quoted in the literature [69], which are usually determined by diffusion from a zinc-containing ambient. **Figure 10** shows a SIMS profile of a zinc-doped GaAs layer sandwiched between undoped GaAs layers; as-grown, and after annealing for three hours at 850°C. A diffusion coefficient of about $1-4 \times 10^{-16}$ cm²/s can be inferred from this profile for a zinc concentration of about 1×10^{19} cm⁻³. This is in contrast to diffusion coefficients as high as 7×10^{-8} cm²/s at 900°C which have been reported for zinc diffusing into the *surface* of a substrate from a zinc-containing ambient [65]. This latter

case gives the so-called *infinite source* boundary condition, in which the surface concentration is constant for the duration of the annealing treatment. Reduced zinc diffusion has also been seen in such structures when the zinc source is removed and the sample re-annealed [64]. (Here the surface concentration is reduced and decreases with time as zinc evaporates from the surface.) The difference between the infinite source case and that of epitaxial growth has often been overlooked in quoting zinc diffusion coefficients.

The low diffusion coefficient for buried zinc means that if the desired profile can be realized, it will not diffuse during the rest of the growth process. The memory effect mentioned previously is present for both DEZn and DMZn, and reduces the abruptness of the Zn profile [66, 67, 69, 70]. This can be seen from the carrier concentration profile [as determined from the electrochemical capacitance-voltage (C-V) measurements] of a buried zinc-doped GaAs layer [69], as shown in Figure 11. For sample 1, there was no growth interruption; for sample 2, there was a ten-minute growth interruption. The growth interruptions corresponded to those used for diodes EB-1 and EB-2, described later. The background level was

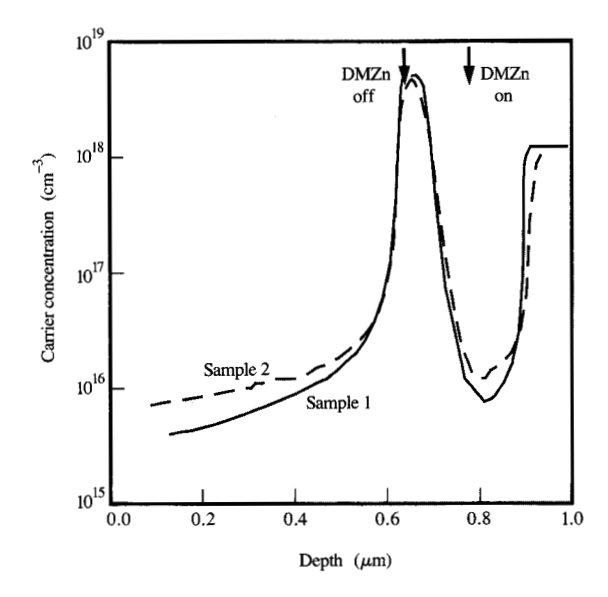


Figure 1

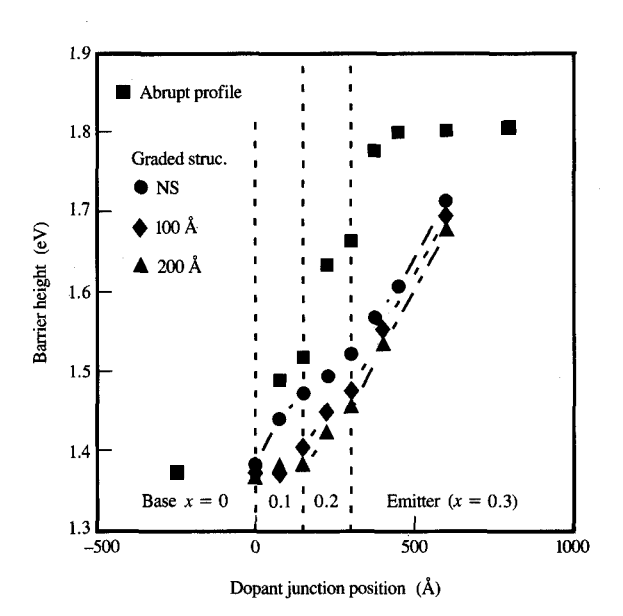
Carrier concentration versus depth of a GaAs structure containing a buried zinc-doped layer. Carrier concentration was determined from electrochemical C-V profiles. Sample 1 had no growth interruption, while Sample 2 had a 10-min growth interruption. These conditions corresponded to those used for diodes EB-1 and EB-2. From [69], reproduced with permission.

slightly lower for sample 1 because it was grown in a cleaner system. Doping transients are clearly seen in both the "turn-on" and "turn-off" of the zinc-doped GaAs layer. The turn-off is much slower than the turn-on, which has important implications for producing heterojunction devices. It is seen that C-V analysis is not sensitive to small changes in the zinc profile resulting from the different growth conditions. The complexity of zinc doping is yet another example of the interdependence of growth and device characteristics. For devices such as semiconductor lasers and solar cells, the p-type layer is grown last. The zinc profile is then determined by the turnon transient, which is quite fast, and an abrupt profile can usually be realized with standard growth conditions. Devices such as npn heterojunction bipolar transistors (HBT) contain a heavily p-type base that is sandwiched between two n-type layers, as shown in Figure 12. The dopant junctions must coincide with the compositional junctions for proper device operation. If this does not occur, a homojunction instead of a heterojunction is formed, and the device characteristics are greatly degraded. The carrier concentration in the HBT must change by more than a factor of 50 in approximately 100 Å for the device to function as designed. The turn-off transient of the zinc between the base and emitter is therefore the critical step in producing functional HBTs.

| 10 2 | |
|--|---|
| $n = 5 \times 10^{18} \text{cm}^{-3}$ | 1500 Å |
| $n = 2 \times 10^{17} \text{cm}^{-3}$ | 1200 Å |
| $n = 2 \times 10^{17} \text{cm}^{-3}$ | 400 Å |
| | 100 Å |
| $p = 5 \times 10^{18} \text{cm}^{-3}$ | 1000 Å |
| | 150 Å |
| $n = 1 \times 10^{17} \text{cm}^{-3}$ | 400 Å |
| $n = 1 \times 10^{17} \text{cm}^{-3}$ | 1200 Å |
| s semi-insulating substrate | |
| | $n = 2 \times 10^{17} \text{ cm}^{-3}$ $p = 5 \times 10^{18} \text{ cm}^{-3}$ $n = 1 \times 10^{17} \text{ cm}^{-3}$ $n = 1 \times 10^{17} \text{ cm}^{-3}$ |

Figure 12

Schematic of the layer structure of an npn heterojunction bipolar transistor having a wide-bandgap emitter and collector. The composition in the grade layers is changed from Al_{0.30}Ga_{0.70}As to GaAs in order to prevent the formation of a spike in the conduction band at the emitter-base junction and at the base-collector junction.



Flaure 13

Calculated barrier heights for an emitter-base (EB) heterojunction diode as a function of dopant-junction position. The position of the dopant junction was assumed to be that at which the donor concentration is equal to the acceptor concentration, measured with respect to the interface between the GaAs and $Al_{0.10}Ga_{0.90}As$ (x=0). The undoped GaAs spacer, if included, was within the base region. The designation NS indicates that no spacer had been employed. From [69], reproduced with permission.

• Abrupt zinc profiles

We have developed an extremely sensitive technique to determine the position of the dopant junction using the electrical characteristics of the heterojunctions themselves [69]. This was necessary because conventional analysis techniques such as SIMS and C-V profiling do not have the sensitivity required to detect the small associated changes in the dopant profile. The barrier height of the junction increases as the dopant profile (in this case Zn) extends through the heterojunction, for example in an HBT, from the base through the graded region and into the wide-bandgap emitter or collector. A p-n homojunction is formed in the high-bandgap material if the acceptor penetrates far enough. The high sensitivity of this electrical transport technique to dopant position is a result of the large change in bandgap with junction position, as seen in Figure 13. This figure shows the calculated change in barrier height for an Al_{0.30}Ga_{0.70}As/GaAs emitter-base junction as the location of the dopant junction moves from the metallurgical junction into the Al_{n 30}Ga_{n 70}As emitter. The dopant junction position was found by comparing the

Table 2 Measured and calculated barrier heights for p-n junctions produced under different growth conditions. Calculated values are for abrupt p-type dopant profiles. Measured values have been scaled by ~0.08 eV to account for inaccuracies in the model and current transport other than thermionic emission [69].

| Junction | Barrier height (eV) | |
|---|---------------------|-------------|
| | Calculated | Measured |
| GaAs homojunction | 1.38 | _ |
| Al _{0.30} Ga _{0.70} As homojunction | 1.81 | _ |
| CB heterojunction | 1.38 | _ |
| EB heterojunction | 1.38 | _ |
| CB | | 1.41-1.43 |
| EB-1 | _ | 1.75 - 1.77 |
| EB-2 | | 1.58 |
| EB-3 | _ | 1.45-1.46 |
| EB-4 | _ | 1.37–1.39 |

effective barrier height, as determined from temperaturedependent current-voltage (I-V) measurements assuming thermionic emission as the dominant current transport mechanism, with barrier heights calculated for structures with realistic dopant profiles. The emitter-base (EB) and collector-base (CB) junctions of Figure 12 were examined separately. The EB junction was used to examine the characteristics of the turn-off transient of the zinc profile; the CB junction was used to examine the turn-on transient. Thin undoped GaAs spacer layers were placed on either side of the base to accommodate a small amount of dopant movement. Measured and calculated barrier heights for several p-n junctions produced under different growth conditions are listed in Table 2. The measured values have been scaled by ~0.08 eV to account for inaccuracies in the model and current transport other than thermionic emission [69]. Measured and calculated barrier heights agreed very well for the collector-base junction CB, in which the turn-on of the zinc dopant is important. The measured I-V characteristics were almost ideal, with an ideality factor of 1 over more than four decades of current. These results indicated that the desired structure could be grown with standard growth conditions. The emitter-base diode EB-1, which was sensitive to the turn-off of the zinc profile, was grown under the same conditions as the collector-base diode CB, yet had very different characteristics. The measured barrier height was 1.75-1.77 eV, which is much larger than the expected value of 1.38 eV. It is, however, very close to the barrier height measured for the Al_{0.30}Ga_{0.70}As homojunction, indicative of significant movement of the zinc out of the base and into the emitter. These transport measurements confirmed the previous conclusion that control of the turn-off of the zinc is the critical step in producing working HBTs.

Diodes EB-2, EB-3, and EB-4 were grown under conditions yielding progressively more abrupt zinc profiles.

As discussed previously, the main cause of the graded zinc profile is the transients associated with the interaction of the dopant precursor with the growth system. These transients are suppressed by reducing the incorporation efficiency of the residual dopant species in the layers grown subsequently. The increasingly abrupt zinc profile is indicated by the systematic decrease in the measured barrier height.

Diode EB-2 had a ten-minute growth interruption between its base and 200-Å-thick undoped spacer. This permitted some of the adsorbed zinc species to be flushed from the system before beginning the growth of the spacer layer. Its barrier height was found to be significantly lower than that for diode EB-1: 1.58 eV as opposed to \sim 1.76 eV. However, it exhibited a large amount of excess recombination current, with no region where the ideality factor was equal to 1 [69]. The excess recombination was probably a result of impurities collecting at the interface during the growth interruption. This dopant junction was located in the $Al_{0.30}Ga_{0.70}As$ layer, as can be seen by comparing the measured barrier height of 1.58 eV to the values in Figure 13.

A better method for producing sharp zinc profiles is to reduce the growth rate in the layer grown after the base, as was done in diode EB-3. This has the effect of compressing the dopant transient toward the intentionally doped layer. The growth rate was reduced by a factor of 6 in the 300-Å-thick spacer. This method results in a further reduction in the barrier height and an improvement in the ideality factor [69]. The dopant junction in diode EB-3 was within the Al_{0.20}Ga_{0.80}As grade layer. Reducing the growth rate is much more effective than simply interrupting the growth. This is evident from the fact that diode EB-3, with 4.3 minutes of growth at a slow growth rate, had a lower barrier height and an ideality factor closer to 1 than diode EB-2, which was grown with a ten-minute growth interruption.

The final method sharpens the turn-off transient by utilizing the reduced incorporation of zinc at higher growth temperatures. The incorporation of zinc decreases dramatically for a relatively small temperature increase, as seen in Figure 9(b). In that case, the base was grown at 650°C, while the subsequent layers were grown at 700°C. This 50°C increase in growth temperature results in almost an order of magnitude decrease in zinc concentration. The temperature increase was completed within the time required to grow the 200-A-thick undoped spacer. There was no growth interruption, and the undoped spacer was again grown at a reduced growth rate. A smaller mole fraction of DMZ (by about a factor of 10) was required to achieve the desired doping level at 650°C, so the total amount of DMZ introduced into the reactor was lower. The measured barrier height was 1.37-1.39 eV, which compares very well to the calculated value of 1.38 eV,

indicating that the diode was the desired heterojunction. These results again show how a knowledge of the growth process points the direction to improving the final structure. In this case abrupt dopant junctions were formed with a dopant (DMZn) which is commonly characterized by a strong memory effect.

Selective epitaxy

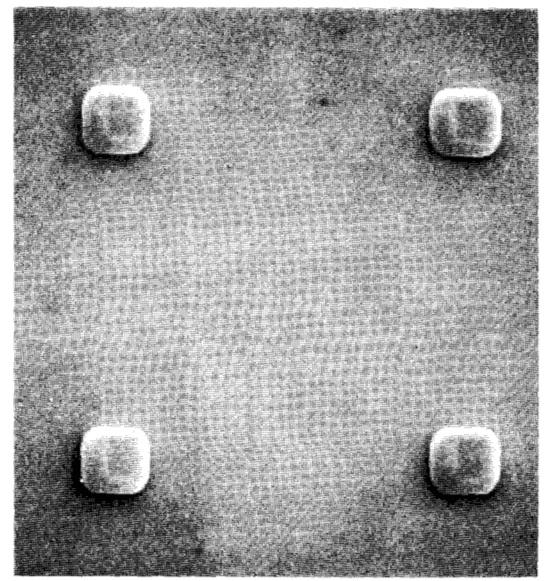
The previous section was concerned with control over the vertical dimensions of the epitaxial structure. Selective epitaxy adds to this control over the lateral dimensions. Selectively deposited material, regrown on patterned epitaxial structures, can provide enhancements for both optical and electronic devices. A MESFET, for example, typically utilizes ion-implanted source-drain contact regions. Lateral straggle of the implanted region under the gate enhances short-channel effects such as gate-lengthdependent threshold voltage, subthreshold leakage, and premature breakdown. Typically, the implanted region is set back laterally from the gate to avoid these problems. However, this causes an undesirable increase in the resistance between the contact and the channel. These concerns become increasingly important as device dimensions, both vertically and laterally, are reduced. Selective epitaxy can alternatively be used to produce selfaligned, shallow contacts. The source-drain regions would be etched down to the channel and refilled, in a selfaligned manner, with heavily doped material. The heavily doped contact region would then be very close to, but not under, the gate. However, the selective regrowth process must meet a number of stringent criteria in order to be useful. These criteria include growth of single-crystal material only within unmasked areas, with no deposition on masked regions. The thickness, morphology, and edge profile must also be controlled. In addition to these structural requirements, the electrical properties of the regrown interface and subsequently formed layers should approach those of conventionally grown material.

Prior work using MOVPE has not met these criteria. The deposition has not been completely selective under typical growth conditions, leaving polycrystalline deposits on the mask material [71]. Additionally, enhanced growth rates occur near the edge of the mask, resulting from surface diffusion of the growth nutrients from the masked to the open region. This transition region at the edge of the mask can serve as a source of defects which then propagate into the bulk of the regrown layer. The growth can be made selective by modifying the growth conditions to achieve a high desorption rate for the Ga species on the mask material. Growth conditions which minimize such deposition on the mask require high growth temperatures, low growth rates, and low pressure. Such conditions are not necessarily conducive to growing high-quality material. A more important consideration for electronic devices is

that the interface between the regrown material and the underlying epitaxial layer is often found to be contaminated by unintentional impurities and deep traps [72]. These interfacial defects, resulting from pre-regrowth processing, limit the utility of selective epitaxy for many applications. A variety of pregrowth surface treatments, using Cl- or Br-based vapor etchants, have been studied in order to reduce these effects [72]. *In situ* vapor etches require the use of temperatures in excess of 800°C to achieve smooth morphologies, which is undesirable because of enhanced diffusion and degradation of materials characteristics often observed at these temperatures.

 Selective epitaxy using diethylgallium chloride The selectivity of the material deposited using MOVPE can be enhanced by using a different growth chemistry, one which exhibits greatly reduced adsorption of the growth precursor on the masking material. We have demonstrated this for the growth of GaAs using diethylgallium chloride, (C,H,),GaCl or DEGaCl, and AsH, [73]. The use of DEGaCl, instead of the more common methyl- or ethyl-based precursors, results in complete selectivity between the open and masked regions of the substrate over a wide range of growth conditions. This is seen in the micrographs in Figure 14, which compare layers deposited onto a partially masked substrate using DEGaCl and TMG. The masking material was Si₃N₄. The large quantity of polycrystalline deposits on the mask resulted from the use of TMG, while no mask deposits were formed when DEGaCl was used. The deposition of GaAs using DEGaCl was completely selective, with a temperature-independent, mass-transport-limited growth rate from 600-750°C. The selectivity was independent of masking material, e.g., silicon dioxide, silicon nitride, and silicon oxynitride, feature size or geometry, or ratio of masked to open areas. Unintentionally doped material, grown at 650°C, was n-type with a carrier concentration of $1-3 \times 10^{15}$ cm⁻³ and a mobility at 77 K of about 32 000 cm²/V-s. Silicon was found to be the dominant donor, while Zn and C were observed as compensating acceptors [73].

Edge profiles for a 1-\mum-thick layer grown at 650°C are shown in the micrographs of Figure 15. The growth rate over the unmasked region was uniform, with no evidence of an enhanced rate at the mask edge, as was observed when TMGa was used. The edges of the selectively grown material were bounded by the slow growth planes of the (110) and (111) type. This was similar to what was found in the inorganically based growth of GaAs using AsCl₃ or HCl. The edge profile was determined by the orientation of the mask opening and the growth temperature. Relatively rough edges can develop, as seen in the micrograph on the right, for which the edges of the mask were not aligned such that the bounding planes of the grown layer



aCl β0 μm

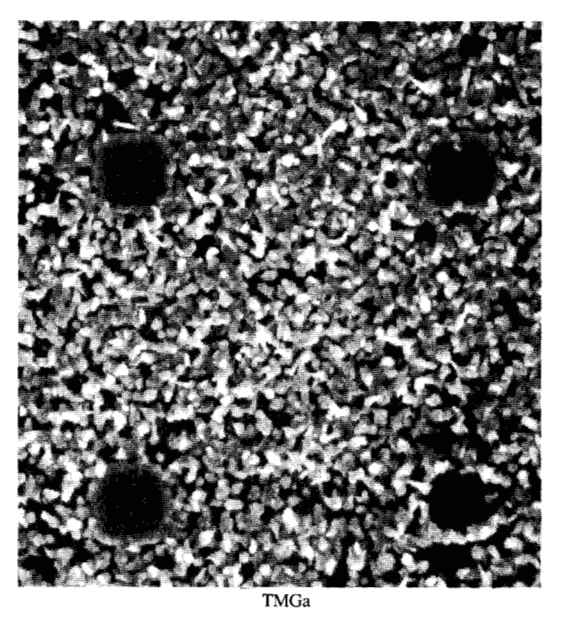


Figure 14

Micrographs of layers deposited onto partially masked substrates, using DEGaC1 and TMGa. The use of DEGaC1 resulted in growth only in the unmasked regions. From [73], reproduced with permission.

intersected the cleavage plane at a right angle. The growth rate was larger on the masked substrates than on unmasked substrates.

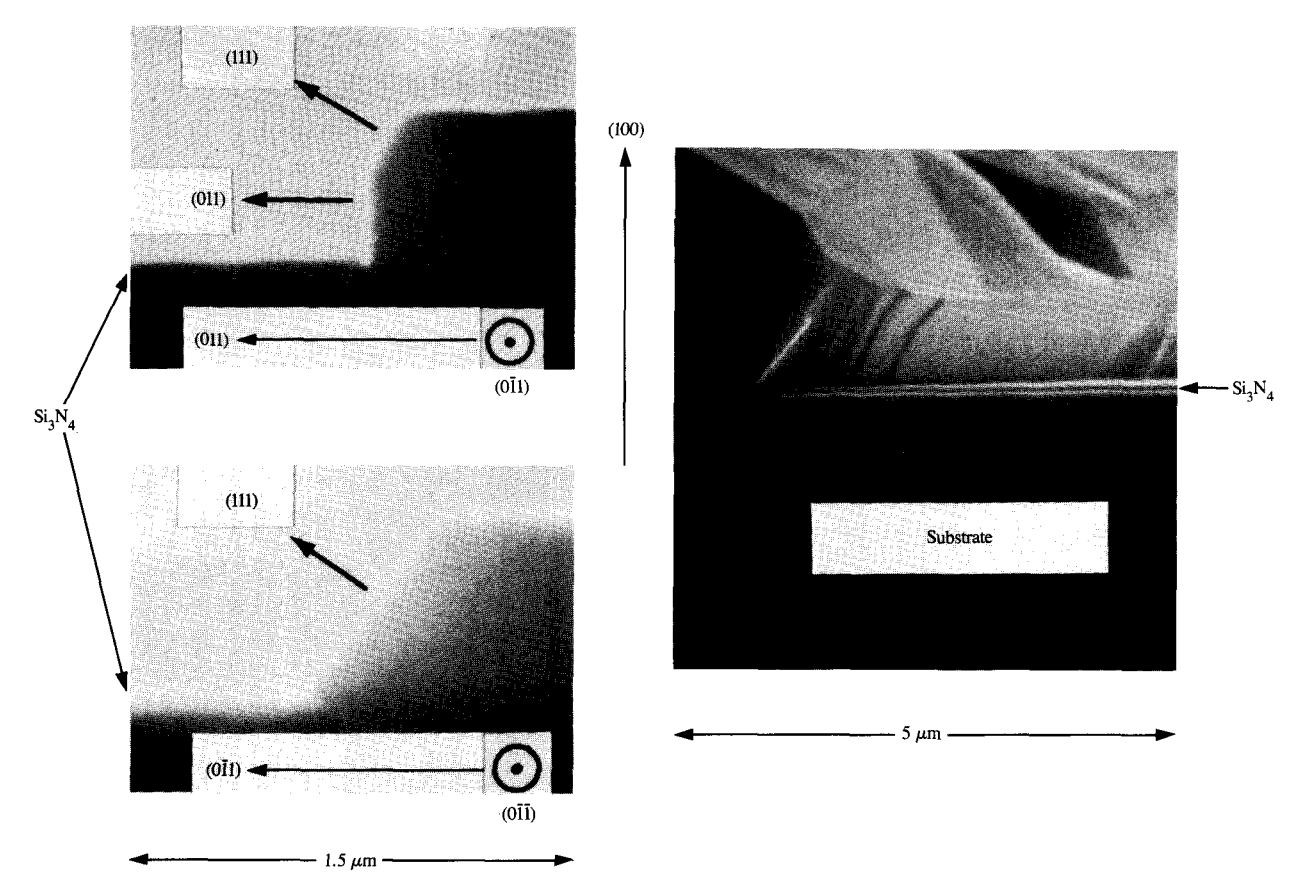
The selectivity observed with DEGaCl using MOVPE is very similar to that observed in inorganically based growth. The *in situ* formation of GaCl from the decomposition of DEGaCl has been suggested as the primary reaction pathway. The formation of GaCl would

explain the similarity to the inorganically based growth. The high supersaturation in the gas phase leads to mass-transport-limited growth. The lack of deposition on the dielectric masking material could be explained by either a high nucleation barrier or very low adsorption of the growth species GaCl. It is unlikely that significant adsorption and diffusion to the mask edges occur, since no growth rate enhancement is observed at the mask edges.

• Electrical characteristics of the regrown interface
In order for the regrowth technique to be useful in a wide range of devices, the electrical properties of the regrown interfaces must approach those of conventionally grown material. The interfaces must be free from defects and significant amounts of charge that could create a potential barrier. Electrical characteristics of regrown interfaces using DEGaCl were thus investigated, first as a function of pre-regrowth surface treatment, and then by contact resistance measurements of regrown contacts to various structures.

The pre-regrowth surface treatment was found to have a large effect on the transport characteristics, with an HCl step necessary to achieve electrically clean interfaces [74]. Three pre-regrowth treatments were applied to identical samples prior to deposition of the DEGaCl-grown top contact. Samples were subjected to (1) no pregrowth treatment; (2) solvent cleaning, ultrasound in acetone and isopropyl alcohol plus water rinse; and (3) solvent cleaning as in (2) followed by five minutes of ultrasound in HCl and a water rinse. The structure that was grown consisted of 1.3 μ m of silicon-doped GaAs (6 × 10¹⁵ cm⁻³) regrown using DEGaCl on top of 2.3 µm of silicon-doped GaAs $(6 \times 10^{16} \text{ cm}^{-3})$. The light doping was used to enhance detection of a potential barrier at the regrown interface. Room-temperature C-V measurements and I-Vmeasurements from 12 to 300 K showed that treatment (3) (solvent cleaning followed by HCl) yielded the best electrical characteristics, i.e., no detectable trap concentrations at or near the interface and linear I-Vbehavior over the entire temperature range.

The contact resistivity across the regrown interface was examined in both the vertical and lateral directions [74, 75]. The contact area in the vertical structure was large, while the lateral contact was more representative of a regrown contact to a thinly doped channel or two-dimensional electron gas. The vertical structures had a 700-Å-thick layer of GaAs grown nonselectively using DEGaCl doped with silicon to a level of 6×10^{17} cm⁻³ on a 2000-Å-thick previously grown GaAs layer doped to a level of 2×10^{17} cm⁻³. The contact resistivity was measured using the transmission-line technique. The contact resistivity ρ_c and sheet resistance R_o of the transmission-line structures obtained at 300 K and 77 K are listed in Table 3. The phosphoric acid + HCl treatment



Micrographs of edge profiles of selectively grown material, using DEGaCl. The profiles depended on the orientation of the mask edges with respect to the substrate. From [73], reproduced with permission.

included a 100-Å-deep etch in $\rm H_3PO_4$: $\rm H_2O_2$: $\rm H_2O$ 2:1:50 followed by 30 s in HCl and a water rinse. This etch was examined because it is commonly used to etch GaAs and AlGaAs in the fabrication of heterostructure devices. The listed values are for the regrown contact itself, having been corrected for the contact resistivity of the contact metallization and the resistance of the 2 \times 10 17 cm $^{-3}$ layer below the regrown layer.

The contact resistivities listed in the table are very low $(2-4\times10^{-7}~\Omega\text{-cm}^2)$, and are near the limit of the accuracy of this technique. The fact that the contact resistivities did not increase at 77 K indicated that a barrier, if present, was very small. An analysis of these results gave a maximum trap concentration at the regrown interface of about $4\times10^{11}~\text{cm}^{-2}$. This confirmed the results from C-V and I-V measurements that the DEGaCl growth chemistry with an HCl pretreatment provides a very clean regrown interface.

Transport through lateral contacts [75] was examined in structures containing a 100-Å-thick GaAs layer doped to a

Table 3 Electrical characteristics of regrown vertical contacts.

| Treatment | Temperature (K) | $R_{\Box} \ (\Omega/\Box)$ | $(\Omega\text{-cm}^2 \times 10^{-7})$ |
|-----------------------|--------------------|----------------------------|---------------------------------------|
| Solvent + HCl | 300 | 60.5 | 3.9 |
| Solvent + HCl | 77 | 53.8 | 2.9 |
| Phosphoric acid + HCl | 300 | 60.4 | 2.3 |
| Phosphoric acid + HCl | 77 | 55.5 | 2.2 |

level of 3×10^{18} cm⁻³, and a two-dimensional electron gas (2DEG) having a sheet density of 7×10^{11} cm⁻². These were patterned as transmission lines with the contact areas etched 500 Å deeper than the conducting layer. The contact areas were then refilled with selectively grown GaAs doped with either Si (3×10^{18} cm⁻³) or Sn (1×10^{19} cm⁻³). Relevant electrical characteristics of these structures are listed in **Table 4**. The contact resistance ρ_c was calculated from the expression $\rho_c = R_c \times w$, where w is the thickness of the n⁺ layer (100 Å). The contact

 Table 4
 Electrical characteristics of regrown lateral contacts.

| Structure + dopant | | T = 300 K | | T = 77 K | | |
|--------------------|----------------------------|--|--|----------------------------------|---|---------------------------------------|
| | $R_{\Box} \ (\Omega/\Box)$ | $R_{\rm c}$ $(\Omega\text{-cm})$ | $\rho_{\rm c}$ $(\Omega\text{-cm}^2)$ | R_{\square} (Ω/\square) | $R_{\rm c}$ $(\Omega\text{-cm})$ | $\rho_{\rm c}$ $(\Omega\text{-cm}^2)$ |
| Lateral:Si | 625 | 4×10^{-3} | 4 × 10 ⁻⁹ | 625 | 4×10^{-3} | 4×10^{-9} |
| Lateral:Sn | 870 | 4.5×10^{-3} | 4.5×10^{-9} | 870 | 4.5×10^{-3} | 4.5×10^{-9} |
| 2DEG:Si 2DEG:Sn | 1250 | 4×10^{-1} | 4×10^{-7} | _ | 4×10^{-1} | 4×10^{-6} 4×10^{-7} |
| 2DEG:Sn (annealed) | 900 1250 | $1.5 \times 10^{-1} \\ 2 \times 10^{-2}$ | $1.5 \times 10^{-7} \\ 2 \times 10^{-8}$ | 860 | $\begin{array}{c} 4 \times 10^{-1} \\ 2 \times 10^{-2} \end{array}$ | $^{4}_{2} 	imes ^{10^{-7}}_{10^{-8}}$ |

resistance was extremely small and independent of temperature, as was the case for the planar contacts. The contact resistance to the 2DEG was much larger and also temperature-dependent. This result could indicate that there is a larger density of traps at the regrown interface in this structure than in the planar or lateral GaAs-only structure.

Computer simulations of this regrown contact to the AlGaAs/GaAs heterostructure were performed to investigate the contact resistance and spatial distribution of carriers for various trap concentrations. A trap concentration of 5×10^{12} cm⁻² between the AlGaAs and regrown GaAs would result in depletion of the 2DEG under the corner of the contact, leading to development of a high contact resistance. This depletion could be greatly reduced by moving the dopant about 200 Å into the channel, i.e., laterally diffusing the dopant into the 2DEG structure. Since tin has a larger diffusion coefficient than silicon, the tin-doped sample was annealed at 850°C for 20 minutes to provide the required lateral diffusion. The contact resistivity (Table 4) was thereby considerably reduced, and became temperature-independent.

Calculations of minimum contact resistivities gave values of about $5 \times 10^{-8} \Omega$ -cm² for $n = 1 \times 10^{17} \text{ cm}^{-3}$ and about $2.5 \times 10^{-9} \Omega$ -cm² for $n = 2 \times 10^{18} \text{ cm}^{-3}$. The experimentally determined contact resistivities were quite close to these values, again indicating the excellent electrical characteristics of the regrown contacts.

Concluding remarks

Currently, the MOVPE technique can be used to deposit virtually any III–V material with good control over its structural and electrical characteristics. The technique has advanced sufficiently that it is being used for the production of many III–V semiconductor devices, most notably lasers, solar cells, and other opto-electronic devices. Electronic devices, such as grown-channel MESFETs and 2DEG structures, require more control of the growth process than is typically achieved in MOVPE. These devices require very fine control over carrier concentration, layer thickness, and interface structure, as well as the ability to repeatably reproduce a given

structure. Indeed, if MOVPE is to become a viable technique for producing a wide range of semiconductor devices, it must become as safe, straightforward, and reproducible as possible. Understanding the basic factors in the growth process which affect the structural and electrical properties of the material produced provides the key to achieving these ends. Experimental investigations of the growth process, as well as more realistic modeling of the entire growth ambient, including its chemical, thermal, and hydrodynamic aspects, will be necessary for the further development of this technique. Such investigations will lead to the use of new precursors or purification techniques to achieve materials of higher purity, and precursors which are less toxic and hazardous. Unique advantages can be realized through the development of new precursors, e.g., the use of DEGaCl to achieve selective epitaxy. An improved understanding of the growth process will certainly lead to better control and increased reproducibility. Additional developments such as atomic layer epitaxy and modulation-enhanced epitaxy are being applied to gain additional control over the growth process. Although MOVPE has advanced considerably in the last two decades, there is clearly potential for significant further progress.

References

- 1. H. M. Manasevit, Appl. Phys. Lett. 12, 156 (1968).
- J. D. Grange, in The Technology and Physics of Molecular Beam Epitaxy, E. H. C. Parker, Ed., Plenum Press, New York, 1985, pp. 47-48.
- J. Nishizawa and T. Kurabayashi, J. Electrochem. Soc. 130, 413 (1983).
- M. G. Jacko and S. J. W. Price, Can. J. Chem. 41, 1560 (1963).
- N. I. Buchan, C. A. Larsen, and G. B. Stringfellow, J. Cryst. Growth 92, 591 (1988).
- 6. M. Yoshida, H. Watanabe, and F. Uesugi, J. Electrochem. Soc. 132, 677 (1985).
- P. W. Lee, T. R. Omstead, D. R. McKenna, and K. F. Jensen, J. Cryst. Growth 85, 165 (1987).
- C. A. Larsen, N. I. Buchan, and G. B. Stringfellow, Appl. Phys. Lett. 52, 480 (1988).
- S. P. DenBaars, B. Y. Maa, P. D. Dapkus, A. D. Danner, and H. C. Lee, J. Cryst. Growth 77, 188 (1986).
- M. Tirtobidjojo and R. Pollard, J. Cryst. Growth 77, 200 (1986).

- K. F. Jensen, D. I. Fotiadis, P. W. Lee, D. R. McKenna, and H. K. Moffat, Growth of Semiconductors, SPIE Proceedings No. 796, March 1987, Bay Point, FL, March 26-27, 1987, p. 150.
- 12. G. B. Stringfellow, J. Cryst. Growth 68, 111 (1984).
- G. B. Stringfellow, Organometallic Vapor-Phase Epitaxy, Theory and Practice, Academic Press, Inc., Boston, 1989.
- F. C. Eversteyn, P. J. W. Severin, C. H. J. v.d. Brekel, and H. L. Peek, J. Electrochem. Soc. 117, 925 (1970).
- 15. F. Rosenberger, Fundamentals of Crystal Growth, Springer, Berlin, 1979.
- Y. Monteil, R. Favre, A. Bekkaoui, P. Raffin, J. Bouix, J. Marcillat, and P. Dutto, J. Cryst. Growth 93, 270 (1988).
- 17. L. Stock and W. Richter, J. Cryst. Growth 77, 144 (1986).
- H. Moffat and K. F. Jensen, J. Cryst. Growth 77, 108 (1986).
- J. E. Williams and R. W. Peterson, J. Cryst. Growth 77, 128 (1986).
- J. Van De Ven, G. M. J. Rutten, M. J. Raaijmakers, and L. J. Giling, J. Cryst. Growth 76, 352 (1986).
- R. B. Bird, W. E. Stewart, and E. N. Lightfoot, Transport Phenomena, John Wiley, New York, 1960.
- 22. T. F. Kuech, Mater. Sci. Rep. 2, 1 (1987).
- D. H. Reep and S. K. Ghandhi, J. Electrochem. Soc. 130, 675 (1983).
- D. H. Reep and S. K. Ghandhi, J. Electrochem. Soc. 131, 2697 (1984).
- T. F. Kuech and E. Veuhoff, J. Cryst. Growth 68, 148 (1984).
- R. Anholt and T. W. Sigmon, J. Electron. Mater. 17, 5 (1988).
- N. Araki-Mishima and K. Yamaguchi, Electron. & Commun. Jpn. Part 2 71, 19 (1988).
- J. W. Matthews and A. E. Blakeslee, J. Cryst. Growth 27, 118 (1974).
- 29. G. C. Osborn, J. Appl. Phys. 53, 1586 (1982).
- C. H. Chen, D. S. Cao, and G. B. Stringfellow, J. Electron. Mater. 17, 67 (1988).
- D. C. Reynolds, K. K. Bajaj, C. W. Litton, P. W. Yu, J. Singh, W. T. Masselink, R. Fischer, and H. Morkoc, Appl. Phys. Lett. 46, 51 (1985).
- M. Tanaka, H. Sakaki, and J. Yoshino, Jpn. J. Appl. Phys. 25, L155 (1986).
- 33. A. Ourmazd, J. Cryst. Growth 98, 72 (1989).
- J. M. Vandenberg, D. Gershoni, R. A. Hamm, M. B. Panish, and H. Temkin, J. Appl. Phys. 66, 3635 (1989).
- (a) T. F. Kuech, E. Veuhoff, T. S. Kuan, V. Deline, and R. Potemski, J. Cryst. Growth 77, 257 (1986). (b) D. P. Kern, T. F. Kuech, M. M. Oprysko, A. Wagner, and D. E. Eastman, Science 241, 936 (1988).
- R. J. Pegler, F. H. Hambleton, and J. A. Hockey, J. Catal. 20, 309 (1971).
- J. D. Parsons and F. G. Krajenbrink, J. Electrochem. Soc. 130, 1780 (1983).
- R. Yakimova, A. P. Roth, D. F. Williams, and V. S. Sundaram, J. Cryst. Growth 68, 71 (1984).
- 39. J. D. Parsons and F. G. Krajenbrink, J. Cryst. Growth 68, 60 (1984)
- T. F. Kuech, M. A. Tischler, R. Potemski, F. Cardone, and G. Scilla, J. Cryst. Growth 98, 174 (1989).
- M. K. Lee, C. Y. Chang, and Y. K. Su, Appl. Phys. Lett. 42, 88 (1983).
- J. P. Duchemin, M. Bonnet, F. Koelsch, and D. Huyghe, J. Electrochem. Soc. 126, 1134 (1979).
- 43. R. Glew, Inst. Phys. Conf. Ser. 63, 581 (1982).
- 44. G. Keil, M. le Metayer, A. Cuquel, and D. le Pollotec, Rev. Phys. Appl. 17, 405 (1982).
- J. J. Yang, L. A. Moudy, and W. I. Simpson, Appl. Phys. Lett. 40, 144 (1982).
- Y.-M. Houng and T. S. Low, J. Cryst. Growth 77, 272 (1986).

- E. E. Wagner, G. Hom, and G. B. Stringfellow, J. Electron. Mater. 10, 239 (1981).
- J. S. Yaun, M. Gal, P. C. Tayor, and G. B. Stringfellow, *Appl. Phys. Lett.* 47, 405 (1985).
- H. K. Moffat, T. F. Kuech, K. F. Jensen, and P.-J. Wang, J. Cryst. Growth 93, 594 (1988).
- J. J. Wang, R. P. Ruth, and H. M. Manasevit, J. Appl. Phys. 52, 6729 (1981).
- J. D. Parsons, L. S. Lichtmann, and F. G. Krajenbrink, J. Cryst. Growth 77, 32 (1986).
- C. R. Lewis, M. J. Ludowise, and W. T. Dietze, J. Electron. Mater. 12, 507 (1983).
- T. F. Kuech, P.-J. Wang, M. A. Tischler, R. Potemski, G. Scilla, and F. Cardone, J. Cryst. Growth 93, 624 (1988).
- M. L. Timmons, P. K. Chiang, and S. V. Hattangady, J. Cryst. Growth 77, 37 (1986).
- T. F. Kuech, M. A. Tischler, P.-J. Wang, G. Scilla, R. Potemski, and F. Cardone, Appl. Phys. Lett. 53, 1317 (1988).
- B. T. Cunningham, M. A. Haase, M. J. McCollum, J. E. Baker, and G. E. Stillman, Appl. Phys. Lett. 54, 1905 (1989).
- B. T. Cunningham, L. J. Guido, J. E. Baker, J. S. Major, Jr., N. Holonyak, Jr., and G. E. Stillman, *Appl. Phys. Lett.* 55, 687 (1989).
- G. Haacke, S. P. Watkins, and H. Burkard, *Appl. Phys. Lett.* 54, 2029 (1989).
- P. W. Lee, T. R. Omstead, D. R. McKenna, and K. F. Jensen, J. Cryst. Growth 93, 134 (1988).
- 60. R. W. Glew, J. Cryst. Growth 68, 44 (1984).
- C. Y. Chang, L. P. Chen, and C. H. Wu, J. Appl. Phys. 61, 1860 (1987).
- 62. B. Tuck, Introduction to Diffusion in Semiconductors, Peter Peregrinus Ltd., England, 1974.
- 63. A. H. van Ommen, J. Appl. Phys. 54, 5055 (1983).
- B. Tuck and A. J. N. Houghton, J. Phys. D: Appl. Phys. 14, 2147 (1981).
- 65. H. C. Casey, in *Diffusion in Semiconductors*, D. Shaw, Ed., Plenum Press, New York, 1973, p. 351.
- P. M. Enquist, J. A. Hutchby, and T. DeLyon, J. Appl. Phys. 63, 4485 (1988).
- 67. P. M. Enquist, J. Cryst. Growth 93, 637 (1988).
- 68. D. G. Deppe and N. Holonyak, Jr., J. Appl. Phys. **64**, R93
- M. A. Tischler, H. Barrate, T. F. Kuech, and P. J. Wang, J. Appl. Phys. 65, 4928 (1989).
- R. W. Glew and M. S. Frost, J. Cryst. Growth 68, 450 (1984).
- H. Hienecke, A. Brauers, F. Grafahrend, C. Plass, N. Putz, K. Werner, M. Weyers, and H. Luth, J. Cryst. Growth 77, 303 (1986).
- T. F. Kuech, E. Marshall, G. I. Scilla, R. Potemski, C. M. Ransom, and M. Y. Hung, J. Cryst. Growth 77, 539 (1986).
- T. F. Kuech, M. A. Tischler, and R. Potemski, Appl. Phys. Lett. 54, 910 (1989).
- M. A. Tischler, T. F. Kuech, A. Palevski, and P. Solomon, *Appl. Phys. Lett.* 55, 2214 (1989).
- A. Palevski, P. Solomon, T. F. Kuech, and M. A. Tischler, Appl. Phys. Lett. 55, 171 (1990).
- M. Yoshida, H. Watanabe, and F. Uesugi, J. Electrochem. Soc. 132, 677 (1985).
- L. M. Yeddanapalli and C. C. Schubert, J. Chem. Phys. 14, 1 (1946).
- W. L. Smith and T. Wartik, J. Inorg. Nucl. Chem. 29, 629 (1967).
- C. A. Larsen and G. B. Stringfellow, J. Cryst. Growth 75, 247 (1986).

Received June 14, 1990; accepted for publication December 11, 1990 Michael A. Tischler IBM Research Division, Thomas J. Watson Research Center, P.O. Box 218, Yorktown Heights, New York 10598. Dr. Tischler is a Research Staff Member in the System Technology and Science Department. He received his B.S. and M.S. degrees in electrical engineering from the University of Michigan in 1978 and 1980. He then worked at the AT&T Bell Laboratories in Allentown, Pennsylvania, in the area of silicon integrated circuits. Dr. Tischler received his Ph.D. in electrical engineering from North Carolina State University in 1986. In that year he joined IBM at the Thomas J. Watson Research Center, where he has worked on crystal growth of III-V compounds by MOVPE and MBE. Dr. Tischler is a member of the American Physical Society and the Institute of Electrical and Electronics Engineers.